


A simple method to reconstruct the molar mass signal of respiratory gas to assess small airways with a double-tracer gas single-breath washout

Johannes Port¹  · Ziran Tao¹ · Annika Junger¹ · Christoph Jopek¹ · Philipp Tempel¹ · Kim Husemann^{2,5} · Florian Singer³ · Philipp Latzin⁴ · Sophie Yammine⁴ · Joachim H. Nagel¹ · Martin Kohlhäuff²

Received: 17 March 2014 / Accepted: 13 March 2017 / Published online: 29 March 2017
© International Federation for Medical and Biological Engineering 2017

Abstract For the assessment of small airway diseases, a noninvasive double-tracer gas single-breath washout (DTG-SBW) with sulfur hexafluoride (SF₆) and helium (He) as tracer components has been proposed. It is assumed that small airway diseases may produce typical ventilation inhomogeneities which can be detected within one single tidal breath, when using two tracer components. Characteristic parameters calculated from a relative molar mass (MM) signal of the airflow during the washout expiration phase are analyzed. The DTG-SBW signal is acquired by subtracting a reconstructed MM signal without tracer gas from the signal measured with an ultrasonic sensor during in- and exhalation of the double-tracer gas for one tidal breath. In this paper, a simple method to determine the reconstructed MM signal is presented. Measurements on subjects with and without obstructive lung diseases including the small airways have shown high reliability and reproducibility of this method.

Keywords Small airway diseases · Double-tracer gas single-breath washout (DTG-SBW) · Signal reconstruction · OLS

1 Introduction

For the examination of lung diseases those characteristic lung function parameters are measured, which primarily reflect the function of the central airways. However, more and more frequently, new techniques and parameters are tested for their capability to assess the status of the small peripheral airways with internal diameters below 2 mm in order to investigate their influence on obstructive lung diseases and other pulmonary conditions [7, 8, 10, 12, 17, 26, 33].

The assessment of small airway dysfunction may be helpful for the therapy of multiple chronic lung diseases in particular with regard to their early detection at a stage before respiratory symptoms arise [3, 4, 11, 22, 30, 31]. Multiple methods and parameters have been developed and proposed [5, 9, 15, 16, 20, 23, 25, 32, 35, 37, 38], but until now, no accepted single method and parameter exists [2, 14].

Recently, a new promising method for the assessment of the small airways with two tracer gases has been developed [27, 28]. Besides oxygen O₂ (21%) and nitrogen N₂ (47.7%), the double-tracer gas additionally contains the two tracer components, sulfur hexafluoride SF₆ (5%) and helium He (26.3%). The concentration of all components in this double-tracer gas mixture is chosen in such a way that its molar mass is about the same as that of medical air. This molar mass range enables optimal signal resolution of the molar mass sensor based on the ultrasonic flowmeter (USFM) principle [28].

One characteristic of this method is that in contrast to multiple-breath-washouts (MBW) only a few respiratory cycles with normal tidal breaths are required. First, some cycles with dry medical air, as it is provided in hospitals,

✉ Johannes Port
jp@bmt.uni-stuttgart.de

¹ Institut für Biomedizinische Technik, Universität Stuttgart, Stuttgart, Germany

² Klinik Schillerhöhe, Zentrum für Pneumologie und Thoraxchirurgie, Robert-Bosch-Hospital, Gerlingen, Germany

³ University Children's Hospital Zurich, Zurich, Switzerland

⁴ University Children's Hospital Basel, Basel, Switzerland

⁵ Internistische Facharztpraxis für Pneumologie, Allergologie, Thoraxonkologie, Bronchoskopie und Schlafmedizin, MVZ Klinikum Kempten GmbH, Kempten, Germany

then one single tidal inhalation of a double-tracer gas mixture, and at the end again one or more cycles with medical air.

Furthermore, recent studies have shown that this method beside the assessment of global ventilation inhomogeneity may also be a sensitive test to assess specific ventilation inhomogeneity in distal airways [1, 13, 18, 25]. It is supposed that this is due to the different diffusion characteristics of both tracers in the convection-diffusion area of the pre-acinar and acinar lung zones which leads to a change of their concentration fractions within the gas mixture.

This new DTG-SBW may have major advantages in contrast to the tidal N_2 -MBW and the vital capacity N_2 -SBW techniques, which are the two principal established test methods. We found that in comparison to the conventional N_2 -MBW the DTG-SBW was on average ten times faster (3 vs. 30 min for three trials) [13]. Compared to the vital capacity N_2 -SBW, which mainly assess the overall ventilation inhomogeneity [34], the DTG-SBW requires only normal tidal breaths and provides information about both, global and peripheral ventilation inhomogeneities.

Thus, the DTG-SBW has major benefits for the patient and hold promise for clinical application [36]. It is especially suitable for elderly and children as it can be performed within a short period of time and only normal tidal breaths are required.

For the analysis, the expiration phase just after the inspiration of the double-tracer gas mixture is used. For that, characteristic parameters are determined from the difference of the molar mass (MM) signals with and without double-tracer gas (Eq. 7), such as its slope between 60 and 90% of the expired volume, which represents the alveolar phase III and reflects consecutive arrival of gas fronts from peripheral diffusion-dependent airways, and its absolute peak at mid-expiratory phase, which represents the bronchial phase II and is determined by the arrival of gas fronts from mainly convection-dependent airways (Fig. 1).

During these expiration phases, however, only the MM signal with the double-tracer gas can be measured. Thus, the MM signal without double-tracer gas has to be reconstructed from the information obtained during previous breaths with medical air.

In this paper a simple method for the calculation of the reconstructed MM signal is presented.

2 Methods and materials

Since no commercially software is available for the signal processing and analysis of the DTG-SBW data, especially not for the reconstruction of the molar mass based

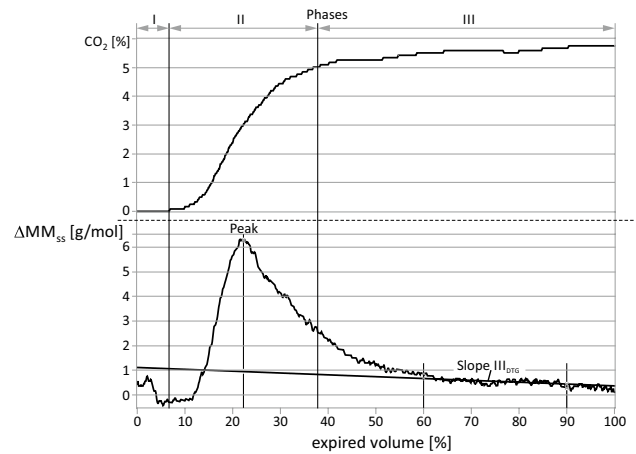


Fig. 1 Typical expirograms of CO_2 and ΔMM_{ss} (Eq. 7) from the dataset of a healthy subject measured with the DTG-SBW. Also shown are peak and slope III_{DTG} (determined between 60 and 90% of the expired volume) which are two characteristic outcome parameters of the DTG-SBW-signal ΔMM_{ss} . The expirograms are partitioned into *phase I* (dead space), *phase II* (bronchial or transitional phase), and *phase III* (alveolar phase)

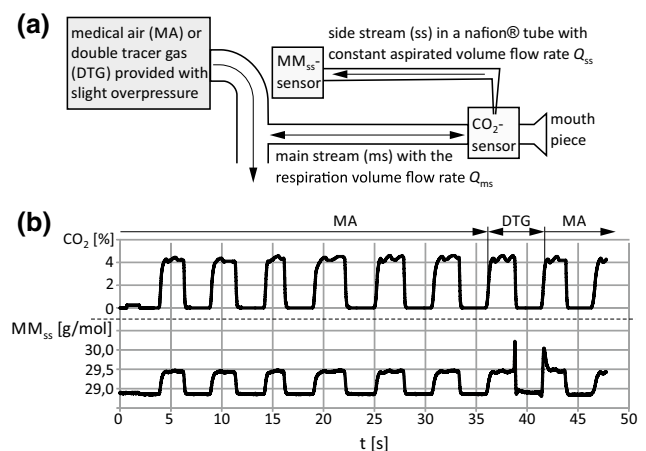


Fig. 2 **a** Schematic measurement setup of those components of the DTG-SBW required for the reconstruction method. **b** MM_{ss} measured in the side stream, and CO_2 -concentration measured in the main stream, both signals are synchronized in time

on our method, we used the software tool LabVIEW™ 2014 version 14.0.1 from National Instruments to write our own software program.

Figure 2 shows a schematic measurement setup of the proposed double-tracer gas single-breath washout (DTG-SBW) and the signals required to understand the reconstruction method. The signals are measured with the commercially available scientific instrument Exhalyzer® D from Eco Medics AG, Duernten, Switzerland, which provides a time resolution of 5ms. The full DTG-SBW and measurement setup are discussed in detail by Singer et al. [28].

During the test, respiratory gas from the main stream is sucked into a side stream with a constant flow rate Q_{ss} of about 3.3 ml/s (Fig. 2). Before the measurement of the molar mass MM_{ss} in this side stream, the gas equilibrates with ambient air conditions (temperature and humidity) by passing it through a nafion[®] tube [19, 21], which is applied for drying respiratory gas [29]. The USFM measurement of the MM is based on the equation for the sound velocity c of an ideal gas

$$c = \sqrt{\frac{RT\gamma}{MM}}$$

where R is the molar gas constant, T the absolute temperature, and γ the adiabatic index. For the evaluation of the MM the sound velocity is determined by measuring the transit times of pulsed ultrasonic waves.

2.1 Reconstruction method

The reconstruction method for the MM signal without double-tracer gas uses the high correlation between that signal and the CO₂-concentration signal [6] during in- and exhalation of dry medical air. For that, the ordinary least squares (OLS) regression method is applied to determine the MM signal from the CO₂-signal. Besides water vapor, which is extracted by the nafion[®] tube, CO₂ is the only remaining component, which is significantly added to the respiratory air during the gas exchange in the lung. Since the CO₂-concentration of the inspired air is very close to zero and therefore negligible, it is only dependent on the internal diffusion process in the respiratory tract and hence not affected by external influences, which is a major advantage. As displayed in Fig. 2b, the MM actually changes almost synchronously with the CO₂-concentration as long as medical air is provided for breathing.

To reconstruct the MM signal, at first, a copy of the measured MM signal is generated. From this copy, all data just after the beginning of the inspiration of the double-tracer gas are deleted. In order to find that beginning, the first spike in the MM signal is detected, which always appears just prior to the start of inspiration of the double-tracer gas mixture. This effect appears to relate to double-tracer gas demixing effects at extremely low flows and continued side-stream sampling. From the remaining signal, the first 25% but not more than 15 s and the last 500 ms are deleted in order to preclude both, artifacts resulting from insufficient sealing of the mouth piece at the beginning of the measurement, and the rise time of the spike, which arises in the transition phase between expiration and inspiration (Fig. 2b). The selected intervals of up to 15 s at the beginning and 500 ms at the end are found to be more than sufficient for a reliable reconstruction of the MM signal.

In the next step, a copy of the CO₂-signal is created and filtered through a digital low-pass filter in order to compensate the observed different time constants between the CO₂- and MM_{ss}-signals at rapid changes of the CO₂-concentration as they occur at the beginning of inspiration. It is thought that dispersion of the respiratory gas during its transmission to the MM_{ss}-sensor within the nafion[®] tube is mainly responsible for these different time constants. From our experimental data, we found a second-order Bessel low-pass filter with a cutoff frequency of 3 Hz and an attenuation greater 20 dB above 12 Hz as the appropriate choice to adapt the time constant of the CO₂-signal to that of the molar mass signal. The Bessel filter is chosen as it preserves the wave shape of the signal in the passband and it allows the estimation of the time delay through the filter, which is important to synchronize the filtered signal CO₂-signal with the other ones. For the reconstruction the same time interval as in the case of the MM signal is extracted from the filtered CO₂-signal.

Since the sensors for the MM and the CO₂-concentration are located at different positions in the measurement setup (Fig. 2a), a time delay between those sensor signals must be taken into account. In fact, we found, that for a given setup that time delay remains almost constant. However, when the setup has been changed, e.g., the nafion[®] tube has been replaced, the time delay may also have changed. Therefore, automatic time synchronization has been implemented in the current reconstruction. For that, the OLS regression coefficients a , b , and ε (Eqs. 4–6) between both signals at different time delays are evaluated by shifting them against each other in the time dimension and using the resulting N pair of values from the overlapping region of both signals to calculate these coefficients. Here, a and b are the vertical intercept and the slope, respectively, of the regression line MM_{sscalc}

$$MM_{sscalc} = a + b \times CO_2, \tag{1}$$

while ε represents the mean squared error between the predicted values MM_{sscalc} and the actual measured values MM_{ss} . With

$$C_{MM_{ss},CO_2} = \sum_i^N (MM_{ss,i} - \overline{MM_{ss}}) \times (CO_{2,i} - \overline{CO_2}) \tag{2}$$

and

$$\sigma_{CO_2} = \sqrt{\sum_i^N (CO_{2,i} - \overline{CO_2})^2} \tag{3}$$

the OLS regression coefficients are estimated as follows:

$$b = \frac{C_{MM_{ss},CO_2}}{\sigma_{CO_2}^2} \quad (4)$$

$$a = \overline{MM_{ss}} - b \times \overline{CO_2} \quad (5)$$

$$\varepsilon = \frac{1}{N} \sum_i^N (MM_{ss,calc,i} - MM_{ss,i})^2 = \frac{1}{N} \sum_i^N \Delta MM_{ss,i}^2 \quad (6)$$

The index i stands for the single measured or predicted values, $\overline{MM_{ss}}$ and $\overline{CO_2}$ are the estimated mean values,

$$\overline{MM_{ss}} = \frac{1}{N} \sum_i^N MM_{ss,i}$$

$$\overline{CO_2} = \frac{1}{N} \sum_i^N CO_{2,i},$$

and $\Delta MM_{ss,i}$ is the error or the so-called residue, i.e., the difference between the predicted and actual value.

In order to limit the computing time, the investigated time delays are restricted to ± 2 s. The time delay, at which the linear regression yields the lowest mean square error ε , is taken for the synchronization of the signals, and the corresponding vertical intercept a and slope b are used for the reconstruction of the MM signal $MM_{ss,calc}$ by means of Eq. (1).

2.2 Evaluation of the goodness of fit

Equation (1) in connection with Eqs. (4) and (5) allows for predicting an MM signal without DTG even in the section where DTG is applied. Such a signal is needed to calculate the relative MM signal ΔMM_{ss} over the whole measurement period by means of

$$\Delta MM_{ss} = MM_{ss} - MM_{ss,calc}, \quad (7)$$

from which the section marked with a dashed circle in the diagrams of Fig. 3 is used for analysis.

In order to evaluate the goodness of the fit, only the time section used for the reconstruction is considered (see the marked section in the diagrams of Fig. 3), since only there measured data values of the MM without DTG are available for comparison.

For this, the mean absolute percent error $\Delta |MM_{ss}^r|$

$$\Delta |MM_{ss}^r| = \frac{1}{N} \sum_i^N \frac{|\Delta MM_{ss,i}|}{MM_{ss,i}} \times 100\%, \quad (8)$$

and the linear correlation coefficient r (Eqs. 2, 3)

$$r = \frac{C_{MM_{ss},CO_2}}{\sigma_{MM_{ss}} \times \sigma_{CO_2}} \quad (9)$$

with

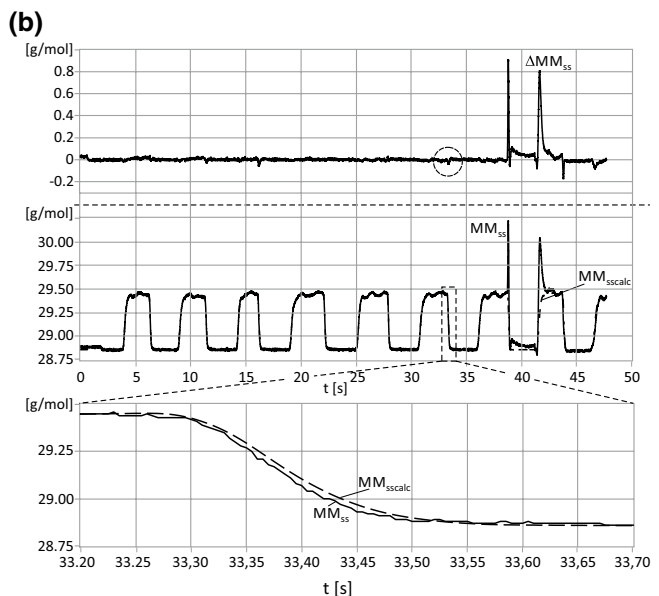
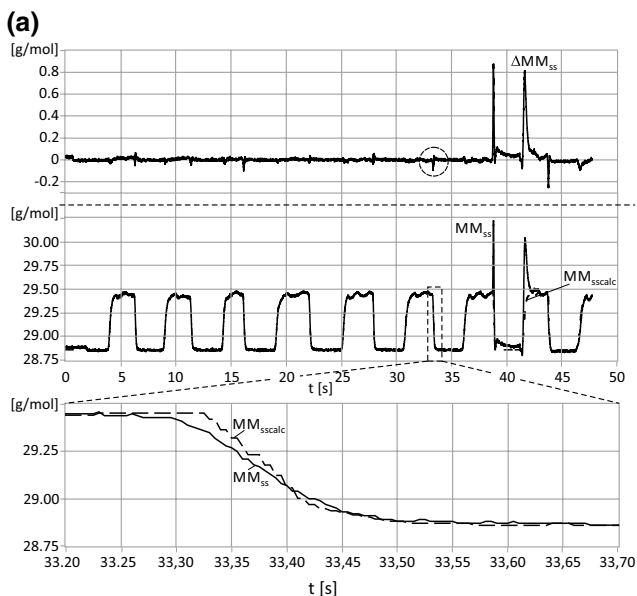


Fig. 3 Reconstructed MM_{ss} -signal with unfiltered (a), and with filtered (b) CO_2 -signal; *top diagrams* ΔMM_{ss} -signal, *middle* measured MM_{ss} - and reconstructed $MM_{ss,calc}$ -signals, *bottom* zoomed section of the *middle diagrams* around the spike marked with a dashed circle in

the *top diagram*. Without the filter, the spikes at the transition from in- to expiration and vice versa are more pronounced due to the dispersion effect and the difference in the respiratory gas mixture during the transition from ex- to inspiration

$$\sigma_{MM_{ss}} = \sqrt{\sum_i^N (MM_{ss,i} - \overline{MM}_{ss})^2},$$

$$\overline{MM}_{ss\text{calc}} = \frac{1}{N} \sum_i^N MM_{ss\text{calc},i},$$

are determined for each of the datasets measured in 92 adult subjects and 60 school-aged children.

From the adult subjects, there have been 35 healthy subjects (HA), 19 with chronic obstructive pulmonary diseases (COPD), 13 with cystic fibrosis (CF), and 25 with asthma (AS). They were measured at the center of pneumology and thoracic surgery at the Robert-Bosch-Hospital, Gerlingen, Germany.

Among the datasets of school-aged children, measured at the University Children’s Hospital of Bern, Switzerland, there have been 18 healthy children (CHA), 21 with cystic fibrosis (CCF), and 21 with asthma (CAS). Of importance, these datasets were not recorded with the software provided by the manufacturer (Spiroware, Eco Medics AG), but with WBreath (3.28, ndd, Zurich, Switzerland).

All subjects performed several tidal DTG-SBW tests per session as part of a large prospective cross-sectional study described in [25, 27]. The tests were approved by the local Ethics Committees. All patients and healthy controls provided full written informed consent. The children’s assent was obtained and all parents or caregivers provided full written informed consent.

All in all, a total of 703 datasets from the 92 adults and 177 from the 60 school-aged children have been available for the determination of the above described goodness of fit parameters for this reconstruction method. From the 703 datasets of adults, 290 came from the group of healthy adults, 198 from the group with COPD, 132 from the group with CF, and 83 from the group with asthma. From the 177 datasets of school-aged children, 47 came from the group of healthy children, 71 from the group with CF, and 59 from the group with asthma.

For a good fit, $\Delta|MM_{ss}^r|$ should be close to zero, r close to 1. $\Delta|MM_{ss}^r|$ close to zero indicates that the expected errors are low and the accuracy of the reconstruction method high. Thus, a correlation coefficient close to 1 and a mean absolute percent error close to zero confirms that the molar mass is well substituted by a linear fit. Since in each case the reconstruction method have to substitute the molar mass with a high accuracy all datasets are used for the evaluation of the goodness of fit.

2.3 Estimation of the respiratory quotient

We also wanted to know, whether our reconstruction method may be applicable for the estimation of the respiratory quotient. For that, we assumed that within the dried respiratory gas only the concentrations of CO₂ and O₂ are significantly changing. Then the MM_{ss} of the dried respiratory gas can be approximated by

$$MM_{ss} \approx MM_{const} + mm_{CO_2} \times CO_2 + mm_{O_2} \times O_2. \quad (10)$$

Here, mm_{CO₂} [0.4401 g/(mol%)] and mm_{O₂} [0.31998 g/(mol%)] are the specific molar masses of CO₂ and O₂, respectively, while MM_{const} represents the MM fraction of all those gas components, in particular nitrogen [≈78%, mm_{N₂} = 0.2801 g/(mol%)] and argon [≈0.9%, mm_{Ar} = 0.39948 g/(mol%)], which are supposed to be constant. Thus, if there really exists a high linear correlation between CO₂ and MM_{ss}, and MM_{const} actually remains constant, then due to Eq. (10), this also leads to a high linear correlation of O₂ to both MM_{ss} and CO₂. In case of the correlation between CO₂ as the independent and O₂ as the dependent variable we have

$$O_2 = o + p \times CO_2, \quad (11)$$

where p and o are the slope and intercept of the regression line. Since o stands for the O₂-concentration at zero CO₂-concentration, this parameter represents the O₂-concentration of the inspired respiratory gas and should therefore be close to 21%.

In order to estimate the respiratory quotient, Eq. (11) is inserted into Eq. (10) and a time derivative is applied to MM_{ss}. Thus, we find

$$\frac{dMM_{ss}}{dt} \approx mm_{CO_2} \frac{dCO_2}{dt} + mm_{O_2} \left(p \times \frac{dCO_2}{dt} \right). \quad (12)$$

Here, the term $p \times (dCO_2)/(dt)$ represents the time rate of change of the O₂-concentration. It has a linear relationship to the time rate of change of the CO₂-concentration with the proportional factor p , whose reciprocal absolute value might be regarded as an estimation of the respiratory quotient (RQ ≈ 1/ p).

To test whether RQ can be estimated from a linear fit between CO₂ and O₂ we evaluated the correlation coefficients by applying our reconstruction method. Additionally we calculated the mean absolute percent error $\Delta|O_2^r|$ of this fit by means of

$$\Delta|O_2^r| = \frac{1}{N} \sum_i^N \frac{|O_{2\text{calc},i} - O_{2i}|}{O_{2i}} \times 100\%, \quad (13)$$

where O_{2calc,i} and O_{2i} represent the reconstructed and measured O₂-value.

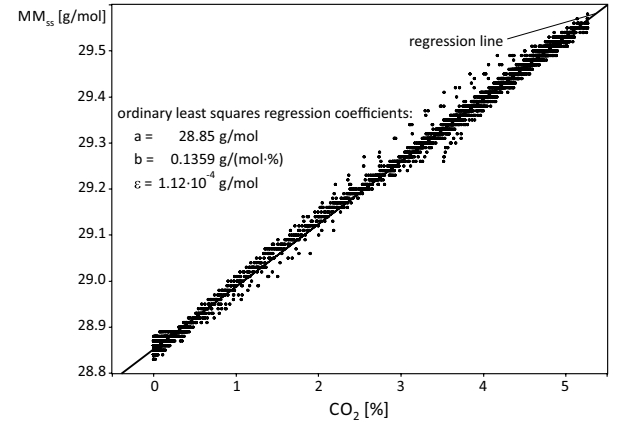
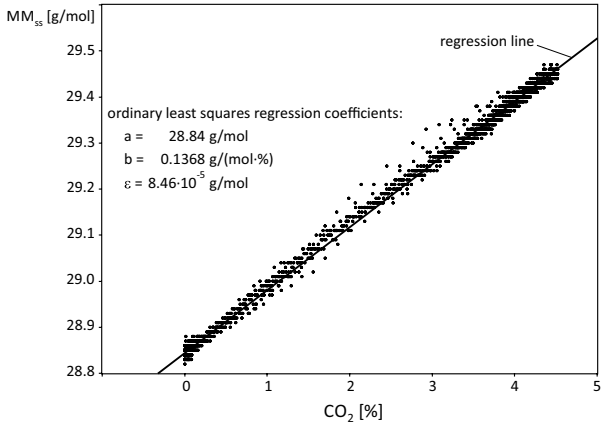
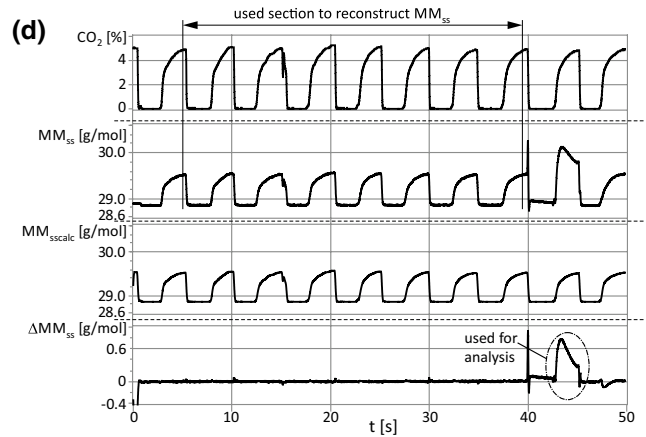
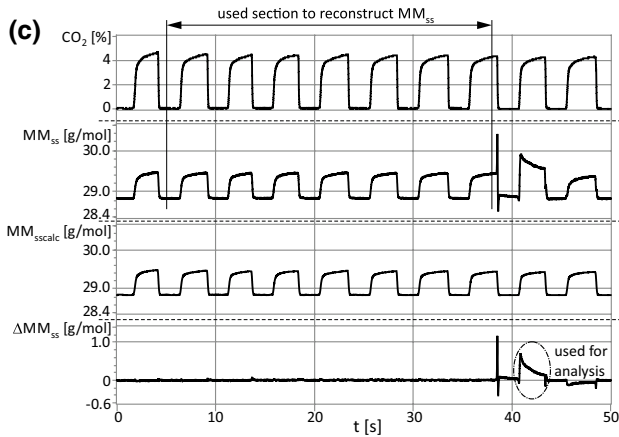
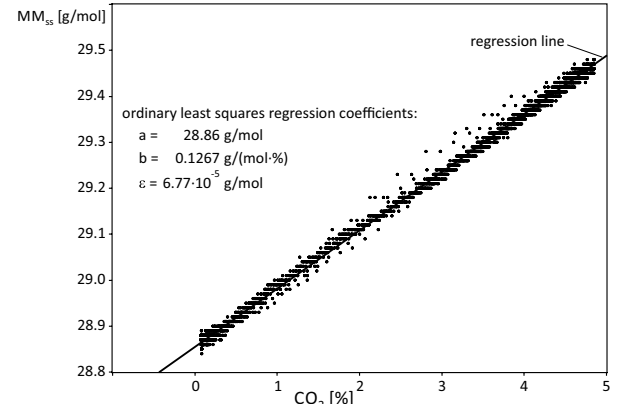
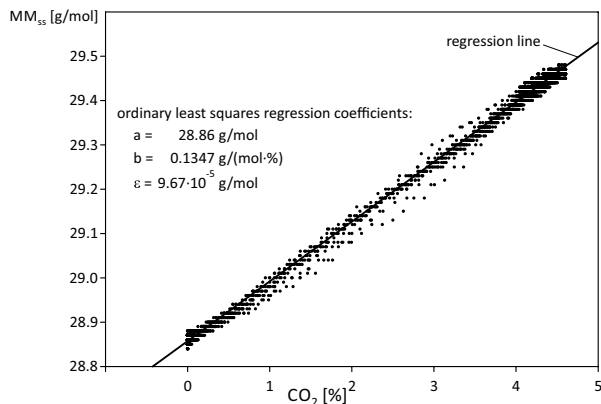
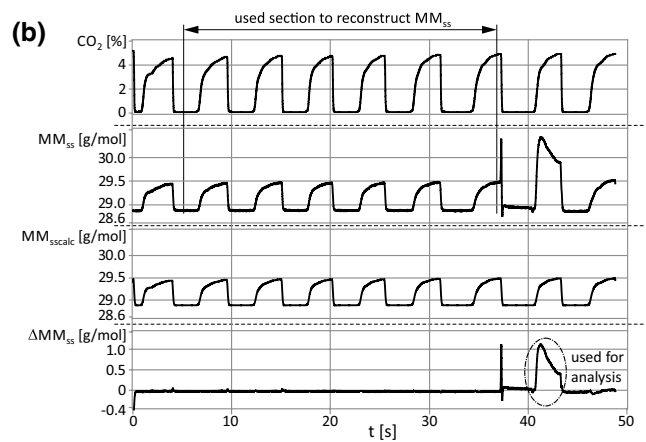
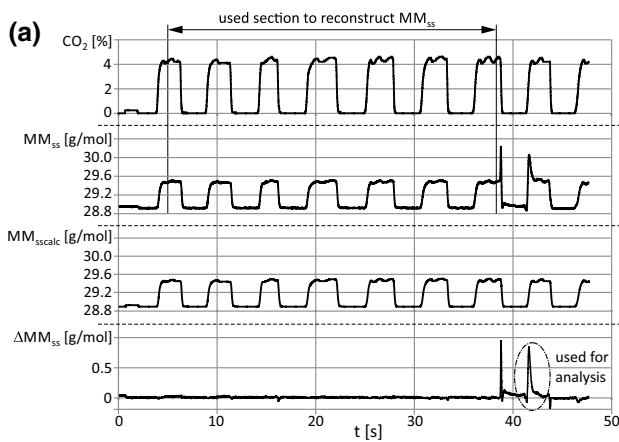


Fig. 4 Scatter plots and time diagrams of healthy (a), COPD (b), asthma (c), and CF (d) adult subjects. The *scatter plots* with CO_2 as the independent and MM_{ss} as the dependent variable use data values taken from the time interval marked in the corresponding time diagrams. In these diagrams, the CO_2 -signal, measured in the main stream, the MM_{ss} -signal, measured in the side stream, the reconstructed $\text{MM}_{\text{sscalc}}$ -signal, and the $\Delta\text{MM}_{\text{ss}}$ -signal as the difference of both MM signals are shown. In *each scatter plot*, the resulting regression line including the regression coefficients are presented

3 Results

Figure 3 displays the influence of the low-pass filter on the quality of the reconstructed signal. The diagrams on the top show the $\Delta\text{MM}_{\text{ss}}$ -signal, in the middle the measured and reconstructed MM_{ss} -signals, and at the bottom a zoomed section of the middle diagram for the sake of a better distinction between the measured and calculated MM_{ss} -signals. In (a) MM_{ss} has been reconstructed with unfiltered in (b) with filtered CO_2 -signal.

As an example for the application of the reconstruction method, Fig. 4 shows the scatter plots and corresponding time diagrams derived from one DTG-SBW test of a HA (a), COPD (b), AS (c), and CF (d) subject, respectively. In the scatter plots, the data values of MM_{ss} and CO_2 taken from the time interval marked in the time diagrams above are displayed. These values are measured from the respiratory gas without DTG and therefore appropriate to determine the OLS regression coefficients to reconstruct the MM_{ss} -signal. The respective regression line and its coefficients as well as the reconstructed MM_{ss} -signal are shown in the scatter plots and time diagrams. The section of the MM_{ss} -signal, which is used for assessing demixing effects of SF_5 and He is marked with a dashed circle.

Table 1 shows the mean values and standard deviations (SD) of the linear regression coefficients and the parameters for the evaluation of the goodness of fit described in Sect. 2.2. They are averaged over all adult subjects as well as over all HA, all COPD, all AS, and all CF subjects. Additionally, for each parameter their range of encountered values is listed.

As an example, Fig. 5 displays the scatter plot and corresponding time diagram derived from a DTG-SBW test of a healthy child. The regression line and regression coefficients are evaluated from the measured CO_2 - and MM_{ss} -values within the time period marked in the time diagram above. Again, the section of the MM_{ss} -signal which is used for the analysis is marked with a dashed circle.

Table 2 presents the same parameters as Table 1, however, this time calculated from the datasets of the children.

As an example for the estimation of RQ, Fig. 6a shows a scatter plot of CO_2 and O_2 including the regression line

and regression coefficients for a healthy subject. They are calculated from the CO_2 - and O_2 -values within the marked section of Fig. 6b, where the CO_2 -, O_2 - and MM_{ss} -signals with end-expiratory and end-inspiratory concentration values for the determination of the respiratory quotients are displayed.

Table 3 lists additionally to the O_2 - and CO_2 -concentrations, which have been found in the different end-expiratory (ee) and end-inspiratory (ei) respiration cycles within the diagram of Fig. 6b, the corresponding evaluated RQ values. The concentration values in this table are given in percent.

Table 4 shows the mean values and standard deviations (SD) of the linear regression coefficients, the parameters for the evaluation of the goodness of fit, and the estimated RQs which result from the datasets of the adults when applying the linear fit between CO_2 and O_2 . Like in Table 1 they are averaged over all adult subjects as well as over all HA, all COPD, all AS, and all CF subjects. Additionally, for each parameter their range of encountered values is listed.

4 Discussion

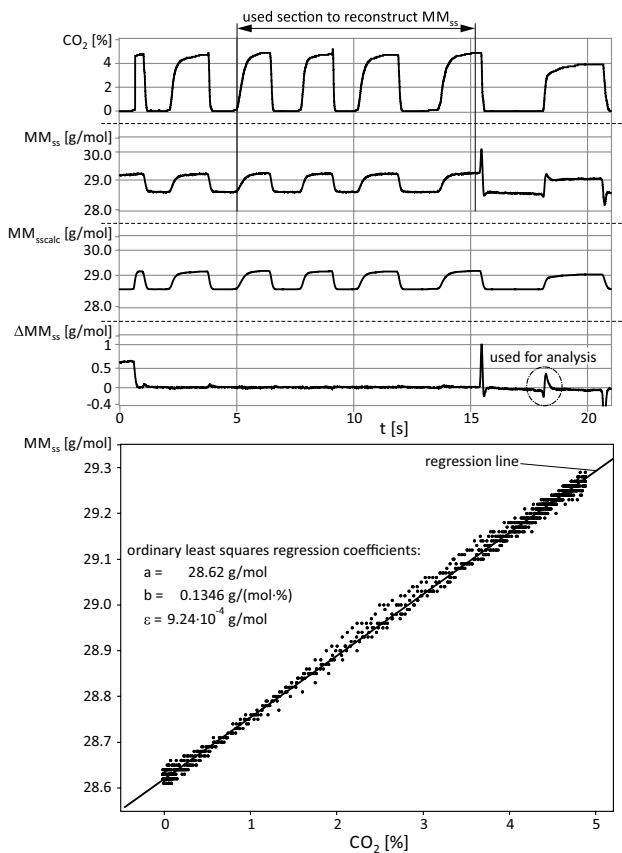
From Fig. 3 it can be seen, that at the transition from in- to expiration, and vice versa, the spikes in the $\Delta\text{MM}_{\text{ss}}$ -signal are less pronounced with than without the filter. The reason for that is that the filter compensates for both the dispersion effect and the slight difference in the respiratory gas mixture measured by the CO_2 - and the MM_{ss} -sensor at the beginning of the inspiration phase, where the subject inspires gas from the dead space formed by the tube of the main stream.

The CO_2 -concentration of the gas is equal to that of the expired gas and, therefore, about 4%. Since the CO_2 -sensor is located at the end of this tube, it measures the CO_2 -concentration of the whole dead space volume, while the MM_{ss} -sensor at the end of the side stream tube receives its gas not quite from the end of that tube. As a consequence, the MM decreases slightly earlier than the CO_2 -concentration, as can be seen in the lower diagram of Fig. 3a. However, this effect does not play any role at the beginning of expiration, since the CO_2 -concentration in the dead space volume of the respiratory tract is about zero. That, in addition with the much more rapidly changing CO_2 -concentration during inspiration, explains why the spikes are more expressed at the transition from expiration to inspiration.

The results in Tables 1 and 2 show that regardless of whether the datasets are from adults or children the proposed method is very well suited for the reconstruction of the MM by means of the CO_2 -concentration.

Table 1 Mean values and standard deviations including their range of encountered values of slope \bar{b} , intercept \bar{a} , correlation coefficient \bar{r} , and mean absolute percent error $\Delta|MM_{ss}^T|$ evaluated from 703 datasets of adults and their groups they belong to

Group of subjects	Slope and intercept		Goodness of fit parameters	
	\bar{b} [g/(mol%)]	\bar{a} (g/mol)	\bar{r}	$\Delta MM_{ss}^T $ (%)
	Mean \pm SD	Mean \pm SD	Mean \pm SD	Mean \pm SD
	min max	min max	min max	min max
All	$0.136 \pm 0.516 \times 10^{-2}$	$28.85 \pm 0.28 \times 10^{-1}$	$0.9993 \pm 0.3407 \times 10^{-3}$	$0.27 \times 10^{-1} \pm 0.47 \times 10^{-2}$
	0.116 0.160	28.78 28.91	0.9939 0.9997	$0.20 \times 10^{-1} 0.79 \times 10^{-1}$
HA	$0.136 \pm 0.470 \times 10^{-2}$	$28.85 \pm 0.24 \times 10^{-1}$	$0.9994 \pm 0.2173 \times 10^{-3}$	$0.27 \times 10^{-1} \pm 0.44 \times 10^{-2}$
	0.124 0.153	28.78 28.89	0.9985 0.9997	$0.21 \times 10^{-1} 0.48 \times 10^{-1}$
COPD	$0.135 \pm 0.549 \times 10^{-2}$	$28.86 \pm 0.29 \times 10^{-1}$	$0.9992 \pm 0.5211 \times 10^{-3}$	$0.26 \times 10^{-1} \pm 0.56 \times 10^{-2}$
	0.124 0.160	28.79 28.91	0.9939 0.9996	$0.20 \times 10^{-1} 0.79 \times 10^{-1}$
AS	$0.136 \pm 0.656 \times 10^{-2}$	$28.85 \pm 0.36 \times 10^{-1}$	$0.9994 \pm 0.1905 \times 10^{-3}$	$0.26 \times 10^{-1} \pm 0.32 \times 10^{-2}$
	0.116 0.156	28.78 28.91	0.9988 0.9997	$0.21 \times 10^{-1} 0.34 \times 10^{-1}$
CF	$0.136 \pm 0.448 \times 10^{-2}$	$28.86 \pm 0.24 \times 10^{-1}$	$0.9993 \pm 0.2609 \times 10^{-3}$	$0.27 \times 10^{-1} \pm 0.43 \times 10^{-2}$
	0.124 0.149	28.79 28.91	0.9982 0.9996	$0.21 \times 10^{-1} 0.41 \times 10^{-1}$

**Fig. 5** Scatter plot with regression line and regression coefficients generated from the CO_2 - and MM_{ss} -values within the time period marked in the time diagrams above, in which the measured and reconstructed signals of a child are shown

The averaged values, standard deviations and range of encountered values for r listed in those tables demonstrate that within each investigated dataset r is very close to 1. This means that even in the worst case there is a very high correlation between the MM and the CO_2 -concentration.

Additionally, the averaged values, standard deviations and range of encountered values for $\Delta|MM_{ss}^T|$ indicate that the values are very well predicted by the reconstruction method, and even in the worst case only a small error is to be expected.

This may suggest that the current method is at least non-inferior compared to the MM_{sscalc} method based on both CO_2 and O_2 -signals [28].

The main outcome parameter for analysis, the slope between 60 and 90% of the expired volume, is only dependent on the shape of the curve. In this case, absolute values of the molar mass are of less importance. However, in cases where absolute values become important, like the absolute peak at mid-expiratory phase or the area under the curve (AUC), a level of error based on clinical significance must be found at which the reconstruction can be identified as failed. Especially the AUC has shown to be of clinical significance [13]. Presently, a reliable level of error for the reconstruction cannot be provided until systematic analysis of the influence of breathing pattern and variations of the tracer gas components on the molar mass signal are available.

Applying the linear regression method for CO_2 and O_2 to all 703 datasets of adults, we get the averaged values and standard deviations of slope and intercept as $\bar{p} = -0.945 \pm 0.107$ and $\bar{o} = 20.92 \pm 0.094$ with a mean absolute percent error of $\Delta|O_2^T| = 0.80\%$. As can be seen, the mean value of o actually lies close to 21%

Table 2 Mean values and standard deviations including their range of encountered values of slope \bar{b} , intercept \bar{a} , correlation coefficient \bar{r} , and mean absolute percent error $\Delta|MM_{ss}^f|$ evaluated from 177 datasets of children and their groups they belong to

Group of subjects	Slope and Intercept		Goodness of fit parameters	
	\bar{b} [g/(mol%)]	\bar{a} (g/mol)	\bar{r}	$\Delta MM_{ss}^f $ (%)
	Mean \pm SD	Mean \pm SD	Mean \pm SD	Mean \pm SD
	min max	min max	min max	min max
CAII	$0.155 \pm 0.791 \times 10^{-2}$	$28.94 \pm 0.28 \times 10^{-1}$	$0.9991 \pm 0.4144 \times 10^{-3}$	$0.33 \times 10^{-1} \pm 0.54 \times 10^{-2}$
	0.141 0.180	28.89 29.00	0.9973 0.9996	$0.24 \times 10^{-1} 0.55 \times 10^{-1}$
CHA	$0.163 \pm 0.865 \times 10^{-2}$	$28.94 \pm 0.22 \times 10^{-1}$	$0.9992 \pm 0.3251 \times 10^{-3}$	$0.32 \times 10^{-1} \pm 0.50 \times 10^{-2}$
	0.151 0.180	28.89 28.98	0.9982 0.9996	$0.27 \times 10^{-1} 0.50 \times 10^{-1}$
CAS	$0.151 \pm 0.515 \times 10^{-2}$	$28.92 \pm 0.26 \times 10^{-1}$	$0.9989 \pm 0.3854 \times 10^{-3}$	$0.35 \times 10^{-1} \pm 0.58 \times 10^{-2}$
	0.141 0.165	28.89 28.98	0.9977 0.9994	$0.24 \times 10^{-1} 0.53 \times 10^{-1}$
CCF	$0.154 \pm 0.528 \times 10^{-2}$	$28.94 \pm 0.28 \times 10^{-1}$	$0.9991 \pm 0.4524 \times 10^{-3}$	$0.32 \times 10^{-1} \pm 0.50 \times 10^{-2}$
	0.141 0.166	28.89 29.00	0.9973 0.9996	$0.25 \times 10^{-1} 0.55 \times 10^{-1}$

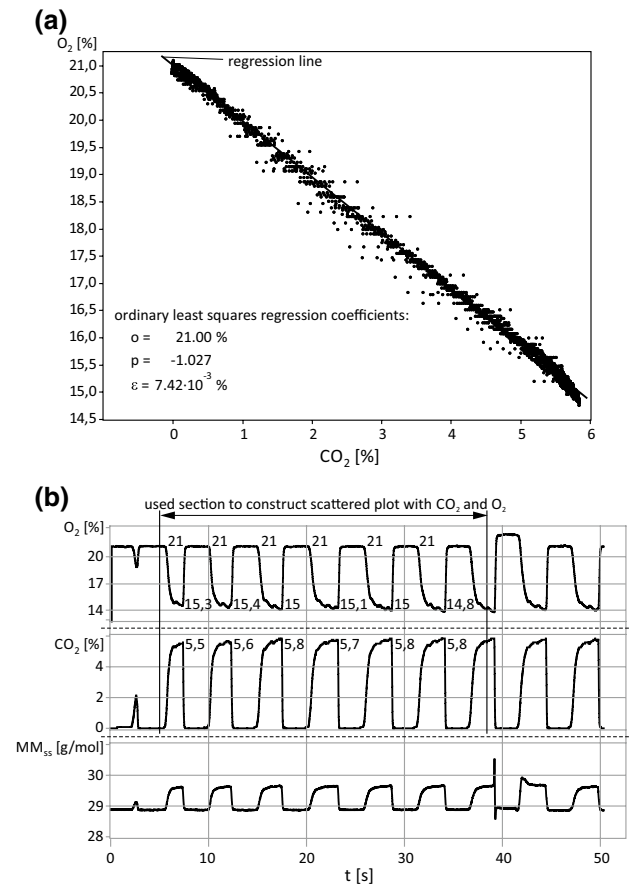


Fig. 6 **a** Scatter plot with regression line and regression coefficients for a healthy subject with CO_2 as the independent and O_2 as the dependent variable. The data values are from the signals shown in the below diagram. **b** CO_2 -, O_2 - and MM_{ss} -signals with end-expiratory and end-inspiratory concentration values for the determination of the respiratory quotient. The concentration values are given in percent

as expected. Inserting Eq. (11) into Eq. (10) and using above mean values, we get

$$MM_{ss} \approx 2891 \text{ g/mol} + 0.138 \text{ g/(mol\%)} \times CO_2. \quad (14)$$

When comparing the intercept and slope values of the regression line described by Eq. (14) with those listed in the first row of Table 2, we find that they are very similar. This means that the regression line described by Eq. (1) does not only represent a pure mathematical fitting but, due to Eq. (10), also a physical approximation.

In case of the regression line shown in Fig. 6 we get a p value of -1.027 which gives an RQ estimate of about 0.973. When calculating the RQ over several respiratory cycles (Table 3) from the same O_2 - and CO_2 -signals (Fig. 6) used for the determination of the regression line, we obtain an average RQ of 0.97, which in fact is very close to the above estimate.

However, the range of encountered values for RQ shown in Table 4 reveals that despite the result found in the example above an overall reliable estimation of RQ was not possible. The values for the regression coefficients and mean absolute percent error as well as the range of encountered values listed in Table 4 show that the O_2 -signal cannot be reconstructed with the same high accuracy like the molar mass signal. In case of MM_{ss} the maximum mean absolute percent error is lower than 0.08%, while in case of O_2 it is almost 3.3%, i.e., about a factor of 41 higher than that of MM_{ss} . We assume that this is the reason why in some cases an unphysiological RQ up to a value of 2 is estimated.

5 Conclusion

Without DTG, there is a high correlation between the CO_2 -concentration and the MM in the dried respiratory

Table 3 O₂- and CO₂- concentration values and the resulting respiratory quotient (RQ). The subscripts ee and ei stand for end-expiratory and end-inspiratory. Within all respiratory cycles it is CO_{2,ei} ≈ 0%. All concentration values are given in percent (%)

	Respiratory cycles					
	1	2	3	4	5	6
O _{2,ei}	21	21	21	21	21	21
O _{2,ee}	15.3	15.4	15	15.1	15	14.8
CO _{2,ee}	5.5	5.6	5.8	5.7	5.8	5.8
RQ	0.97	1	0.97	0.97	0.97	0.94

Table 4 Mean values and standard deviations including their range of encountered values of slope \bar{p} , intercept \bar{o} , correlation coefficient \bar{r} , mean absolute percent error $\Delta|O_2^T|$, and estimated RQ as a result

from the linear fit between CO₂ and O₂. They are evaluated from 703 datasets of adults and their groups they belong to

Group of subjects	Slope and Intercept		Goodness of fit parameters		Estimated RQ
	\bar{p}	\bar{o} (%)	\bar{r}	$\Delta O_2^T $ (%)	\bar{RQ}
	Mean ± SD	Mean ± SD	Mean ± SD	Mean ± SD	Mean ± SD
	min max	min max	min max	min max	min max
All	-0.953 ± 0.107	20.94 ± 0.92 × 10 ⁻¹	0.9971 ± 0.5132 × 10 ⁻²	0.54 ± 0.26	1.06 ± 0.14
	-1.333 -0.454	20.65 21.70	0.9246 0.9996	0.19 3.01	0.75 2.20
HA	-0.959 ± 0.109	20.94 ± 0.89 × 10 ⁻¹	0.9976 ± 0.2932 × 10 ⁻²	0.54 ± 0.27	1.06 ± 0.13
	-1.225 -0.552	20.65 21.21	0.9630 0.9996	0.23 1.82	0.82 1.81
COPD	-0.950 ± 0.105	20.95 ± 0.10	0.9963 ± 0.8478 × 10 ⁻²	0.53 ± 0.29	1.07 ± 0.15
	-1.166 -0.454	20.73 21.70	0.9246 0.9993	0.21 3.06	0.86 2.20
AS	-0.976 ± 0.125	20.93 ± 0.85 × 10 ⁻¹	0.9977 ± 0.2724 × 10 ⁻²	0.50 ± 0.21	1.05 ± 0.18
	-1.333 -0.490	20.71 21.10	0.9846 0.9996	0.19 1.15	0.75 2.04
CF	-0.928 ± 0.875 × 10 ⁻¹	20.94 ± 0.83 × 10 ⁻¹	0.9965 ± 0.2714 × 10 ⁻²	0.60 ± 0.21	1.09 ± 0.11
	-1.164 -0.685	20.77 21.22	0.9859 0.9995	0.23 1.31	0.86 1.50

gas. This is a prerequisite for the DTG-SBW test to correct for naturally exhaled CO₂ and extract the SF₆-He washout behavior. This method allowed us to reconstruct the MM without DTG, by means of the OLS regression method, even if DTG is applied. Our results showed that this method is applicable to datasets of both healthy subjects and subjects with COPD, CF and asthma. However, a reliable estimation of the respiratory quotient with that method appears to be impossible.

We have also demonstrated that this method is applicable to datasets measured from children. Thus, the proposed reconstruction method fulfills all requirements to become the standard method of choice within the DTG-SBW, since it is simple and has a high reliability and reproducibility. The use of a standard reconstruction method have major implications for the clinical practice, since it avoids variability within the datasets coming from different reconstruction methods, and it makes the datasets comparable among each other.

Although the DTG-SBW has major advantages for the patients, as it is fast and easy to perform and provides the assessment of both, the global and peripheral ventilation inhomogeneities, there are still some challenging questions,

which has to be answered before it will be accepted within the clinical practice. Related to the reconstruction method presented in this paper, a reliable level of error must be found which are based on the clinical acceptance and therefore indicate that the reconstruction failed.

Such a level of error could be also used within the clinical application as online control during the measurement. Since the reconstruction could already be started short after a few respiration cycles with medical air, a threshold for the mean absolute percent error, for instance, could be used to indicate, that the measurement must be interrupted due to a maybe weak sealing of the mouthpiece or insufficient functioning of the nafion[®] tube.

References

1. Abbas C, Singer F, Yammine S, Casaulta C, Latzin P (2013) Treatment response of airway clearance assessed by single-breath washout in children with cystic fibrosis. *J Cyst Fibros* 12(6):567–574
2. Boeck L, Gensmer A, Nyilas S, Stieltjes B, Re TJ, Tamm M, Latzin P, Stolz D (2016) Single-breath washout tests to assess small airway disease in COPD. *Chest* 150:1091–1100

3. Burgel PR (2011) The role of small airways in obstructive airway diseases. *Eur Respir Rev* 20(119):23–33
4. Contoli M, Kraft M, Hamid Q, Bousquet J, Rabe KF, Fabbri LM, Papi A (2012) Do small airway abnormalities characterize asthma phenotypes? In search of proof. *Clin Exp Allergy* 42(8):1150–1160
5. Diong B, Rajagiri A, Goldman M, Nazeran H (2009) The augmented RIC model of the human respiratory system. *Med Biol Eng Comput* 47(4):395–404
6. Granstedt F, Folke M, Ekström M, Hök B, Bäcklund Y (2005) Modelling of an electroacoustic gas sensor. *Sens Actuators B Chem* 104(2):308–311
7. Green K, Buchvald FF, Marthin JK, Hanel B, Gustafsson PM, Nielsen KG (2012) Ventilation inhomogeneity in children with primary ciliary dyskinesia. *Thorax* 67(1):49–53
8. Gustafsson PM (2007) Peripheral airway involvement in CF and asthma compared by inert gas washout. *Pediatr Pulmonol* 42(2):168–176
9. Gustafsson PM, Ljungberg HK, Kjellman B (2003) Peripheral airway involvement in asthma assessed by single-breath SF₆ and He washout. *Eur Respir J* 21(6):1033–1039
10. Gustafsson PM, Robinson PD, Lindblad A, Oberli D (2016) Novel methodology to perform sulfur hexafluoride (SF₆)-based multiple-breath wash-in and washout in infants using current commercially available equipment. *J Appl Physiol* 121:1087–1097
11. Hamid Q (2012) Pathogenesis of small airways in asthma. *Respiration* 84(1):4–11
12. Hansen J (2008) Assessing small airways disease. *Eur Respir J* 32(5):1410 (author reply 1410–1410; author reply 1411)
13. Husemann K, Berg N, Engel J, Port J, Joppek C, Tao Z, Singer F, Schulz H, Kohlhäufel M (2014) Double tracer gas single-breath washout: reproducibility in healthy subjects and COPD. *Eur Respir J* 44(5):1210–1222
14. Husemann K, Haidl P, Kroegel C, Voshaar T, Kohlhäufel M (2012) Lung function diagnostics for the small airways. *Pneumologie* 66(5):283–289
15. Kelly VJ, Brown NJ, King GG, Thompson BR (2010) A method to determine in vivo, specific airway compliance, in humans. *Med Biol Eng Comput* 48(5):489–496
16. Latzin P, Thamrin C, Kraemer R (2008) Ventilation inhomogeneities assessed by the multibreath washout (MBW) technique. *Thorax* 63(2):98–99
17. Lombardi E, Hall GL, Calogero C (2013) Pulmonary function testing in infants and preschool children. In: Eber E, Midulla F (eds) *ERS handbook of paediatric respiratory medicine*. European Respiratory Society, Lausanne
18. Nyilas S, Singer F, Kumar N, Yammine S, Meier-Girard D, Koerner-Rettberg C, Casaulta C, Frey U, Latzin P (2016) Physiological phenotyping of pediatric chronic obstructive airway diseases. *J Appl Physiol* 121:324–332
19. O'Rourke C, Klyuzhin I, Park JS, Pollack GH (2011) Unexpected water flow through Nafion-tube punctures. *Phys Rev E Stat Nonlin Soft Matter Phys* 83(5 Pt 2):056,305
20. Robinson PD, Latzin P, Verbanck S, Hall GL, Horsley A, Gappa M, Thamrin C, Arets HGM, Aurora P, Fuchs SI, King GG, Lum S, Macleod K, Paiva M, Pillow JJ, Ranganathan S, Ratjen F, Singer F, Sonnappa S, Stocks J, Subbarao P, Thompson BR, Gustafsson PM (2013) Consensus statement for inert gas washout measurement using multiple- and single-breath tests. *Eur Respir J* 41(3):507–522
21. Rohani M, Pollack GH (2013) Flow through horizontal tubes submerged in water in the absence of a pressure gradient: mechanistic considerations. *Langmuir* 29(22):6556–6561
22. Shaw RJ, Djukanovic R, Tashkin DP, Millar AB, du Bois RM, Orr PA (2002) The role of small airways in lung disease. *Respir Med* 96(2):67–80
23. Shi Y, Aledia AS, Tatavoosian AV, Vijayalakshmi S, Galant SP, George SC (2012) Relating small airways to asthma control by using impulse oscillometry in children. *J Allergy Clin Immunol* 129(3):671–678
24. Singer F, Abbas C, Yammine S, Casaulta C, Frey U, Latzin P (2014) Abnormal small airways function in children with mild asthma. *Chest* 145(3):492–499
25. Singer F, Houltz B, Latzin P, Robinson P, Gustafsson P (2012) A realistic validation study of a new nitrogen multiple-breath washout system. *PLoS ONE* 7(4):e36,083
26. Singer F, Kieninger E, Abbas C, Yammine S, Fuchs O, Proietti E, Regamey N, Casaulta C, Frey U, Latzin P (2013) Practicability of nitrogen multiple-breath practicability of nitrogen multiple-breath washout measurements in a pediatric cystic fibrosis outpatient setting. *Pediatr Pulmonol* 48(8):739–746
27. Singer F, Stern G, Thamrin C, Abbas C, Casaulta C, Frey U, Latzin P (2013) A new double-tracer gas single-breath washout to assess early cystic fibrosis lung disease. *Eur Respir J* 41(2):339–345
28. Singer F, Stern G, Thamrin C, Fuchs O, Riedel T, Gustafsson P, Frey U, Latzin P (2011) Tidal volume single breath washout of two tracer gases—a practical and promising lung function test. *PLoS ONE* 6(3):e17,588
29. Tøien Ø (2013) Automated open flow respirometry in continuous and long-term measurements: design and principles. *J Appl Physiol* 114(8):1094–1107
30. Tulic MK, Christodouloupoulos P, Hamid Q (2001) Small airway inflammation in asthma. *Respir Res* 2(6):333–339
31. Ueda T, Niimi A, Matsumoto H, Takemura M, Hirai T, Yamaguchi M, Matsuoka H, Jinnai M, Muro S, Chin K, Mishima M (2006) Role of small airways in asthma: investigation using high-resolution computed tomography. *J Allergy Clin Immunol* 118(5):1019–1025
32. Usmani OS, Barnes PJ (2012) Assessing and treating small airways disease in asthma and chronic obstructive pulmonary disease. *Ann Med* 44(2):146–156
33. van den Berge M, ten Hacken NHT, Cohen J, Douma WR, Postma DS (2011) Small airway disease in asthma and COPD: clinical implications. *Chest* 139(2):412–423
34. Van Muylem A, Baran D (2000) Overall and peripheral inhomogeneity of ventilation in patients with stable cystic fibrosis. *Pediatr Pulmonol* 30(1):3–9
35. Veiga J, Lopes AJ, Jansen JM, Melo PL (2012) Fluctuation analysis of respiratory impedance waveform in asthmatic patients: effect of airway obstruction. *Med Biol Eng Comput* 50(12):1249–1259
36. Verbanck S, Paiva M (2015) Dual gas techniques for peripheral airway function: diffusing the issues. *Eur Respir J* 45(5):1491–1494
37. Yammine S, Latzin P (2013) Single- and multiple-breath washout techniques. In: Eber E, Midulla F (eds) *ERS handbook of paediatric respiratory medicine*. European Respiratory Society, Lausanne
38. Yammine S, Nyilas S, Casaulta C, Schibli S, Latzin P, Sokollik C (2016) Function and ventilation of large and small airways in children and adolescents with inflammatory bowel disease. *Inflamm Bowel Dis* 22:1915–1922



Dr. Port is senior lecturer at the Institute of Biomedical Engineering. His main research interests are in the fields of biomedical instrumentation, physiological modeling, bioimpedance analysis, and respiratory measurement.



Philipp Tempel received his M.S. degree in Engineering Cybernetics from the University of Stuttgart in 2013. He is currently a Ph.D. student in the field of modeling and simulation of cable-driven parallel robots.



Ziran Tao received his M.S. degree in mechanical engineering at the University of Stuttgart in 2012. His main research interests are data acquisition and signal processing.



Dr. Husemann senior physician in a center of respiratory Medicine, is an expert in the field of pulmonary lung function testing. Her research focus is on inert gas washout testing as noninvasive tool to diagnose small airway diseases.



Annika Junger is a master student in mechanical engineering at the University of Stuttgart. Her fields of study are focused on design engineering and biomedical technology.



Florian Singer is a fellow in Alexander Moellers paediatric pulmonology team at the University Childrens Hospital Zurich, Switzerland. He did a Ph.D. in lung physiology including training in biostatistics and public health.



Christoph Jopek M.S., is head of the electronic engineering division at the Institute of Biomedical Engineering. His main research interests are in the field of ultrasound, biomedical instrumentation, and biosignal processing.



Dr. Latzin is Professor for Paediatric Pulmonology at the University Children's Hospital of Basel since 2013. His major research interests include the developmental physiology of children with and without lung diseases.



Dr. Yammine received her M.D. degree at the University of Bern in 2008. In 2012, she qualified as a pediatrician. Since 2011, she is a research fellow in the Pediatric Pulmonology of the University of Bern, and will apply for her Ph.D. degree.



Prof. Kohlhäuff M.D., is Chief of the Division of Pulmonary Medicine at the Robert-Bosch-Hospital since 2007. His main research interests are focused on aerosol medicine, bronchial carcinoma, and COPD.



Dr. Nagel is Professor and Chairman of the Institute of Biomedical Engineering at the University of Stuttgart since 1996. From 1986 until 1996 he was Professor of BME, Radiology and Clinical Psychology at the University of Miami.